Odgerel et al., 2022. Mongolian Geoscientist 27 (55)
https://doi.org/10.5564/mgs.v27i55.2310

Mongolian Geoscientist

Original Article

Geochronology and Petrogenesis of the Gol Mod Massif: Implications for the Geodynamic Evolution of the Orkhon-Selenge Belt, Northwestern Mongolia

Dashdorjgochoo Odgerel[1*], Bayaraa Ganbat[1,3], Viktor Antipin[2], Dorjgochoo Sanchir[1], Choinbol Tumurchudur[4]

[1*]*Department of Magmatism and Metallogeny, Institute of Geology, Mongolian Academy of Sciences, Ulaanbaatar 18080, Mongolia*
[2]*Vinogradov Institute of Geochemistry, Siberian Branch of the Russian Academy of Sciences, Russian Academy of Sciences, Irkutsk 650033, Russia*
[3]*CAS Key Laboratory of Crust-Mantle Materials and Environments, University of Science and Technology of China, Hefei 230026, China*
[4]*Gurvantalst LLC, Ulaanbaatar 13380, Mongolia*

**Corresponding author: odgereld@mas.ac.mn,, ORCID: 0000-0002-2275-4941*

ARTICLE INFO

***Article history*:**
Received 14 October, 2022
Revised 26 December, 2022

ABSTRACT

The Orkhon-Selenge Belt is a Late Permian to Early Triassic volcanic plutonic belt located in northern Mongolia and is part of the Central Asian Orogenic Belt. The Selenge Complex, which is a part of the Orkhon-Selenge Belt, is a key area for studying the tectonic and magmatic evolution of the Central Asian Orogenic Belt. This study aims to contribute to understanding of the geodynamic evolution of the Orkhon-Selenge Belt by investigating the petrology, geochemistry and geochronology of the rocks in the region. Our results indicate that intrusive rocks were characterized as high-K, Calc-alkaline series and metaluminous to weakly peraluminous I-type granite affinities and their geochemical characteristics are indicating as arc-like geochemical signatures with depleted in elements such as Nb, Ta, Ti and Y and enriched in elements such as Rb, Cs, Th, K and light rare earth elements. Using zircon U-Pb dating, we determined an age of 257.3±0.73 Ma for the alkali granite, suggesting that south-western part of the Orkhon-Selenge Belt formed during the Late Permian time. The Selenge pluton, which is closely related to Erdenet-Ovoo porphyry type mineralization, is a composite intrusion. However, the zircon grains display magmatic and low oxygen fugacity conditions, which characteristics are likely the effect of weak mineralization of magma ascent with Late Permian tectonothermal event in the south-west part of the Orkhon-Selenge Belt. The results of this study will provide insights into the formation and evolution of the north-western segment of the Mongol-Okhotsk Belt, and will have implications for our understanding of the tectonic history of this region.

Keywords: Late Permian; Volcanic plutonic belt; Zircon; Ce^{4+}/Ce^{3+}, Low oxygen fugacity; Selenge Complex

INTRODUCTION

The CAOB hosts a number of large batholiths formed during the Paleozoic and Mesozoic, which are formed in the various geological environments, and the most interesting products of this magmatism are granitoid batholiths of the Late Paleozoic-Early Mesozoic age due to their unique size and role during the late evolution of CAOB (Yarmolyuk et al., 2016) (Fig. 1a). The Orkhon-Selenge Belt is a Late Permian to Early Triassic volcanic plutonic belt located in north western Mongolia and is part of the Central Asian Orogenic Belt (CAOB). The Permian-Triassic volcano-plutonic belt (Badarch

et al., 2002), related to the subduction of Mongol-Okhotsk and Paleo-Tethys oceanic plates under the Siberian continent (Zonenshain et al., 1990; Zorin, 1999). During the Late Paleozoic to Mesozoic, the Mongol-Okhotsk Ocean was closed and subducted northward beneath the Siberian craton (Watanabe and Stein, 2000; Gerel et al., 2005; Windley et al., 2007). Southward subduction of the Mongol-Okhotsk Ocean plate is represented by subduction-related Permian–Jurassic magmatic rocks in the Amur Block (e.g., Tang et al., 2016; Zhao et al., 2017). Northward subduction of the Mongol-Okhotsk Ocean plate was documented by the Middle Carboniferous to Triassic Orkhon -Selenge volcanic plutonic belt and the Angar-Vitim granitoids in Transbaikalia.

The volcanic and plutonic rocks of the Selenge Complex are of particular interest to geologists because they provide a window into the processes that occur during subduction and magmatic activity. For example, the composition of the rocks can be used to reconstruct the composition of the subducted oceanic crust and the mantle wedge, and to understand the processes that led to the formation of the volcanic arc.

In addition to its scientific importance, the north

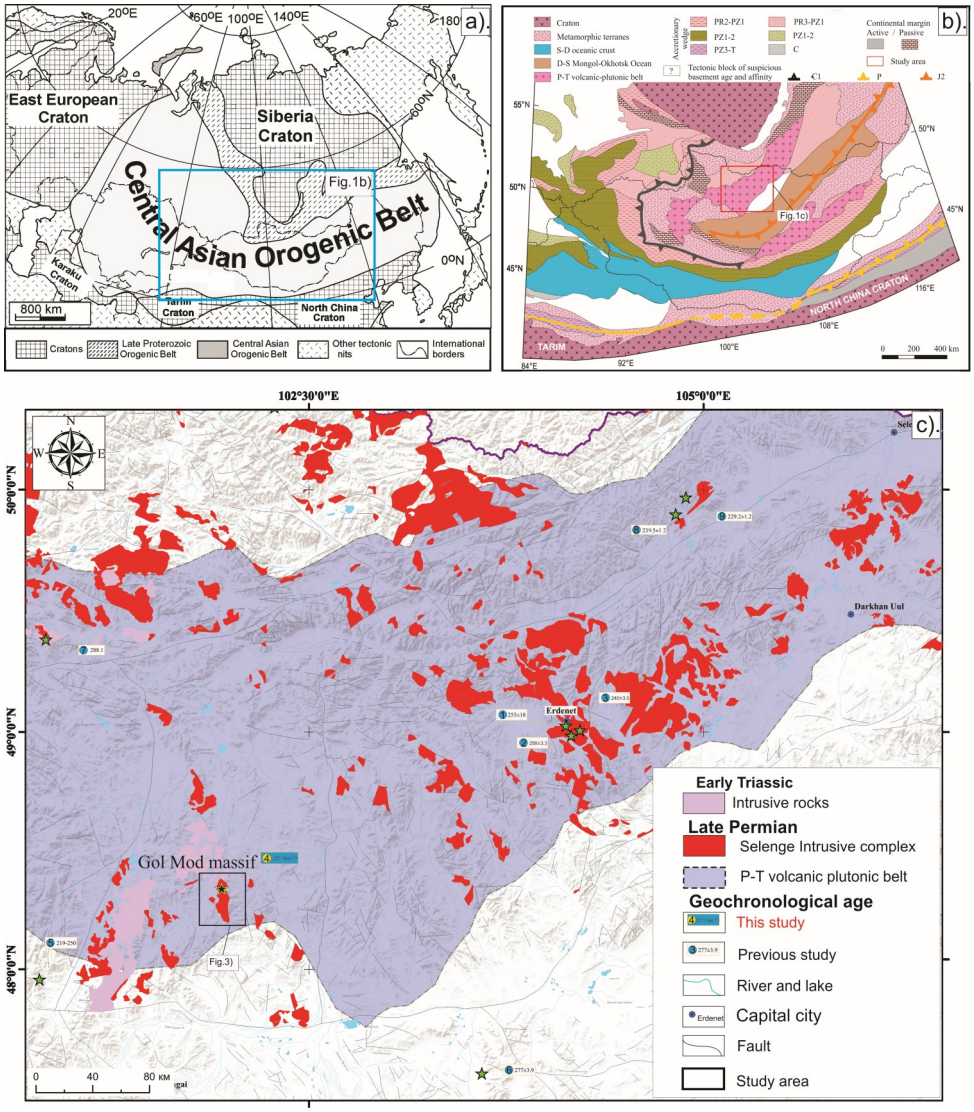

Fig. 1. a) Tectonic outline of CAOB, modified from Şengör et al. (1993) and Jahn et al. (2000) , b) Geological position of Mongolia in the frame of CAOB, modified from Hanžl et al. (2020), c) Late Paleozoic granitoid description in Central and Northeastern Mongolia, Geological map 1:500 000 scale. The shaded area outlines the Permian-Triassic volcanic-plutonic belt, modified from Badarch et al. (2002) and Hanžl et al. (2020)

-eastern part of the Selenge Complex is economically significant because it contains a number of mineral deposits, including copper, gold, and molybdenum (Erdenet-Ovoo porphyry deposit). The Selenge Complex is an important geological feature of north-western Mongolia that provides insights into the processes that occur during subduction and magmatic activity. The complex has both scientific and economic significance, and its study is important for understanding the geology and resources of this region.

The Gol Mod massif is located in the south-western part of the Orkhon-Selenge Belt trough included in the Selenge Complex, the largest volcanogenic structure of the rift zone of the Permo-Triassic North Mongolian magmatic area (Badarch et al., 2002; Berzina and Sotnikov, 2007) (Fig. 2b).

In this paper, we analyzed the geochronology and whole rock and zircon geochemical feature of Gol Mod massif of the south-western part of the Selenge Complex, which have significant implications for magmatic and geodynamic evolution.

GEOLOGICAL SETTINGS

The northern Mongolia is located in a geodynamically complex region, where several tectonic plates converge and interact. The region is characterized by a complex network of faults, folds, and volcanic centers, which reflect the ongoing geodynamic processes in the area.

The Gol Mod massif is located along the northeastern margin of Khangai pluton and the Orkhon-Selenge trough, the largest structure of the Late Paleozoic-Early Mesozoic Northern Mongolian volcano-plutonic belt (Fig. 1c).

The Orkhon-Selenge Belt stretches for approximately 500 kilometers from the western part of Mongolia to its northeastern border with Russia. It is characterized by a series of volcanic and plutonic rocks that were formed through the process of subduction, in which one tectonic plate moves under another. The Selenge Complex is composed mainly of rocks of three associations: first stage-alkaline gabbroid (gabbro and gabbro-diorite), second stage-medium to coarse grained granitoids (biotite and porphyritic, hornblende, alkaline feldspar granites and granodiorite) and final stage-fine to medium grained biotite leucogranites (Tumurchudur et al., 2012). In this study, the Gol Mod massif is illustrated for the second stage of the Upper Permian the Selenge Complex that is composed as alkali feldspar granite and granodiorites (Figs. 2a, b). The granitoid rocks intruded the Lower Permian Khustai formation, Middle Permian Tulbur formation and Late Permian Selenge Complex subvolcanic rocks. Therefore, the Gol Mod intrusive is crosscut by the Middle Triassic Donj Complex and the Upper Jurassic Tsetserleg Complex, and covered by Late Neogene Bod formation and Quaternary sediments (Fig. 3). The geological relationships between the

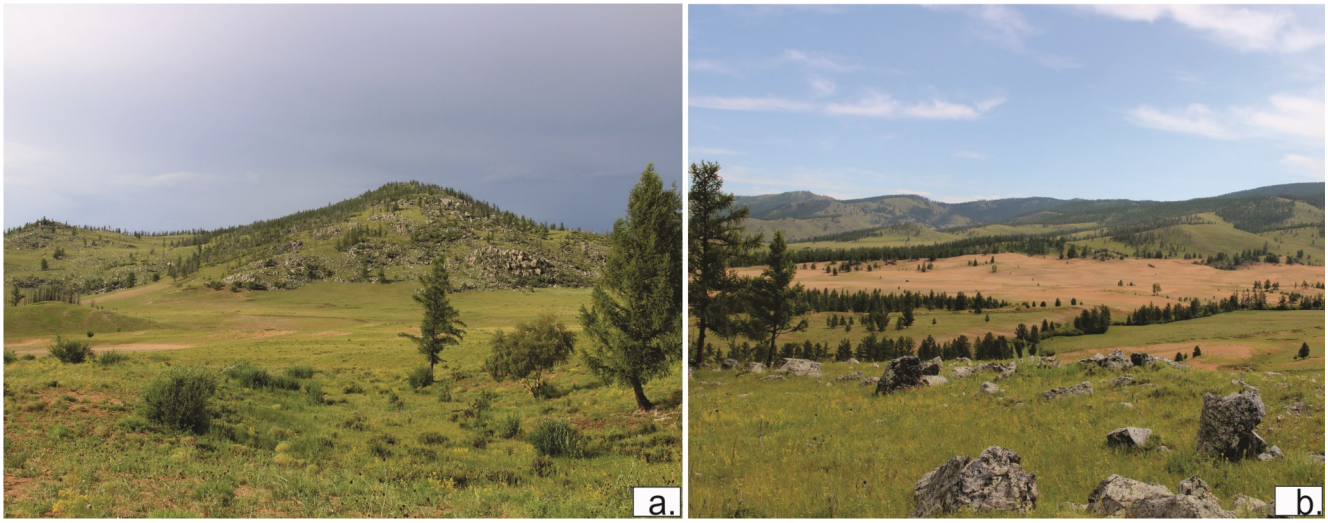

Fig. 2. General overview area of the Gol Mod massif. a) Outcrops of Gol Mod massif; b) Overview of the northwestern part of the Gol Mod massif

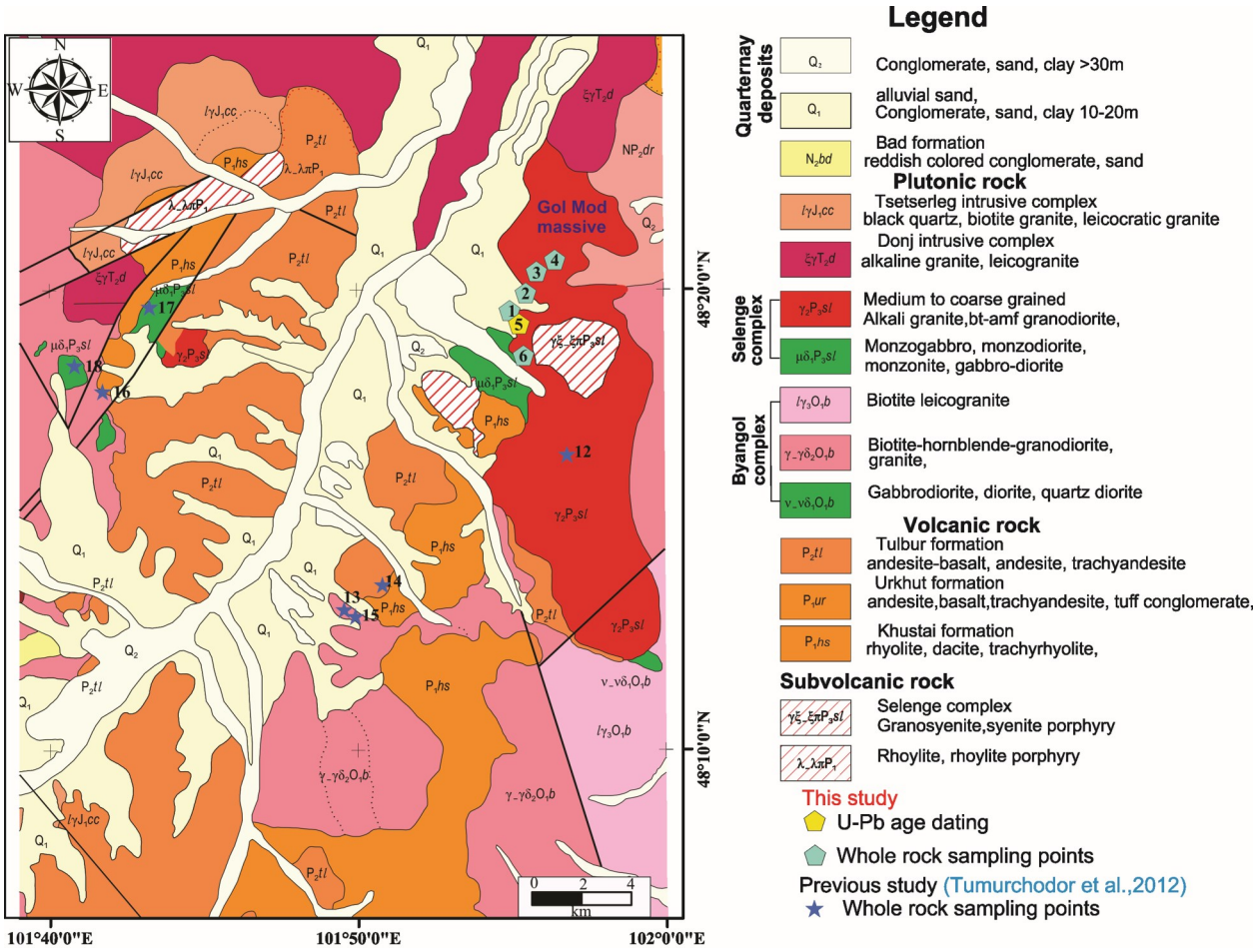

Fig. 3. Geological map of the Gol Mod massif, modified from UGZ-200 scale 1: 200 000 (Gurragchaa and Tomurtogoo, 2014)**.** Geochemical sampling points (from 12 to 18) from (Tumurchudur et al., 2012) and (from 1 to 6) from this study

intrusive rocks of these associations are clear, cutting contacts, and there are no gradual transitions which show evidence of a time gap between the intrusions of their parental melts.

ANALYSES

Sample Selection and Petrography

We collected >10 representative samples distributed over the Gol Mod massif, Central Mongolia. Samples were analyzed for petrography, major and trace element geochemistry, and zircon age dating. For the petrographic study, thin sections were performed by using a microscopy at the Institute of Geology, Mongolian Academy of Sciences.

Characteristic feature of the main minerals assemblages, alongside their accessory minerals phases in the mainly alkali feldspar granite of the study area (Figs. 4a, b).

Alkali feldspar granite: Microscopic studies of the samples (GM-05, 06) showed that they are subsolvus (Fig. 4c). Quartz grains are strained with marked domains of different extension angles. There is an indication of evidence of silica metasomatism as the relative increase in the modal proportion of quartz; with granophyric and myrmekitic textures from a micrographic intergrowth of quartz in K-feldspar and albite with grain size varying largely from 4.5 to 0.25 mm (Fig. 4d). Perthites often occur with narrow rims of small albite laths along crystal interfaces (Fig. 4e). Primary polysynthetically twinned plagioclase feldspar crystals are slightly altered to sericite. Haloes were observed in some biotite crystals which were presumed to be caused by alpha-particle bombardment from small zircon crystals containing radioactive materials with grain size

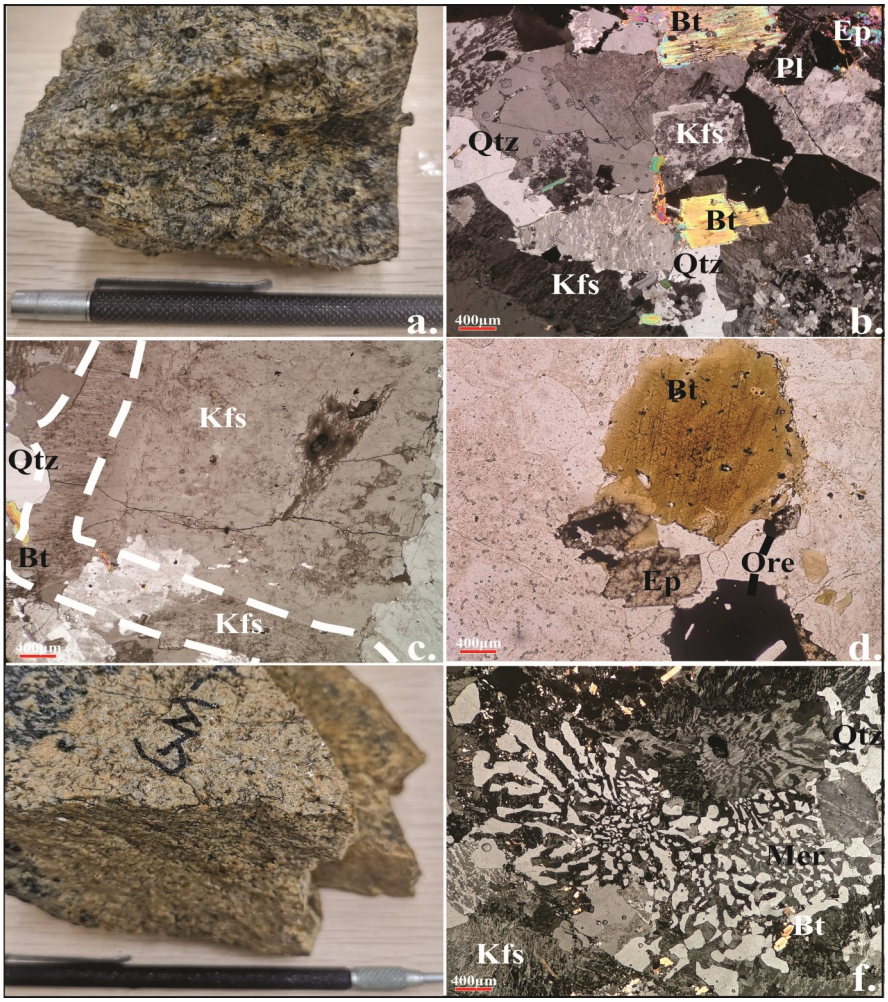

Fig. 4. Photographs of the samples from the Gol Mod massif, Selenge Complex. a. and b.) hand specimens, c–f.) under microscope, c, d, e.) cross-polarized, f.) open-polarized. a) porphyritic biotite-alkali feldspar granite (GM-05), b) medium grained biotite granite (GM-06). Mineral abbreviations are Kfs-feldspar, Pl-plagioclase, Qtz-quartz, Bt-biotite, Ep-epidote, Ap-apatite and Ore-ore minerals.

varying largely from 1.0 to 0.02 mm (Fig. 4f). The volumetrically dominant K-feldspar crystals (60-65%), quartz (15-20%), plagioclase (10-15%), and biotite (10-15%). The minor and accessory minerals in the granites include epidote, chlorite, zircon, apatite, and titanite.

LA-ICPMS zircon U-Pb isotopes

The zircon grains were initially selected by heavy liquid separation and then purified with a magnetic separation technique. The remaining grains were then handpicked under a binocular microscope. The picked zircons were embedded in an epoxy resin and half-sectioned. All mounted grains were photographed under an optical microscope with both reflected and transmitted light to reveal surface flaws and internal inclusions. Finally, they were subjected to cathodoluminescence (CL) to reveal internal textures enabling us to choose target spots for further U-Pb dating. The CL imaging was carried out with a Quanta 200 FEG Scanning Electron Microscope in the SEEL lab of Peking University. Zircon U-Pb analysis was performed at the Key Laboratory of Orogeny and Crust Evolution (Peking University) using a LA-ICP-MS system with a 193-nm ArFExcimer laser and an Agilient 7500c ICP-MS. NIST 610 and Si were used as external and internal standards to calibrate zircon analyses. The Zircon Plesovice (337 Ma) and 91500 standards were used to correct for U-Pb isotope fractionation effects and to monitor the age measurement deviation, respectively. The calculation of

element concentrations and isotopic ratios was performed with GLITTER software (ver.4.4.2) designed by Macquarie University. For common lead correction, we follow the Andersen (2002) method. The Concordia ages were calculated using Isoplot /Excel (3.0), with the weighted mean ages at 95% confidence level (Ludwig, 2003).

Whole rock geochemical analyses

The whole rock chemical analysis including major, trace, and rare earth element (REE) contents, was undertaken at the Center of Isotope-Geochemical Studies, Vinogradov Institute of Geochemistry, Russian Academy of Sciences, Siberian Branch (IGS SB RAS). The samples were homogenized by fusion with lithium metaborate ($LiBO_2$) in an induction furnace in glassy carbon melting pot at 1100°C. The ratio of sample to flux was 1:2. The calibration was carried out using SH1A (granite, Russia), SG-2 (granite, Russia), and JG-2 (granite, Japan) standards. The silicate analyses were performed using a classical chemical method and XRF with inaccuracy 0.5 to 5%. Alkaline elements were analyzed by flame photometry with the precision 5–10%. The trace and elements of rare earth were defined using the ICP-MS method (σ ± 5–10%), with inaccuracy 10–20%. All analyses were done at the Analytical Center for Collective Use, Irkutsk Science Center SB RAS with the use of equipment installed at Center for Collective use, and certified reference samples (Govindaraju, 1994).

RESULT

Major element compositions

The whole-rock geochemical data of the Gol Mod massif are presented in Table 1. Also, analyses of major elements analyses compiled from previous work (Tumurchudur et al., 2012)

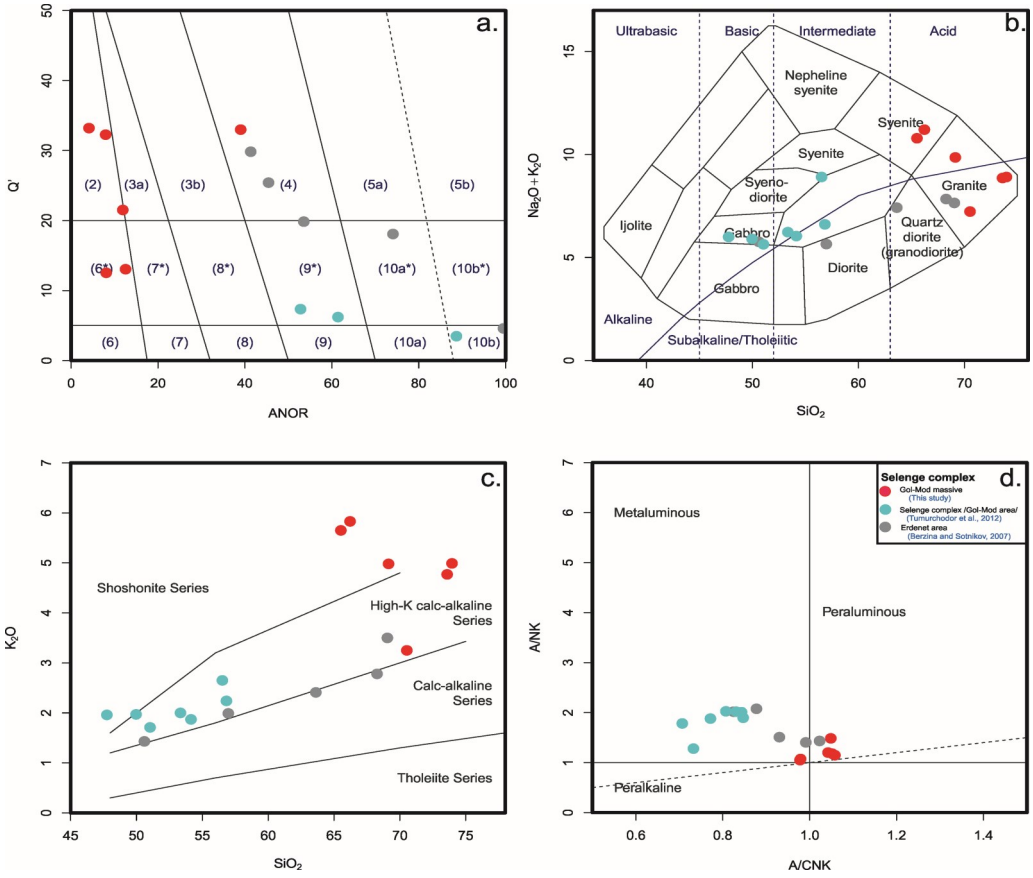

Fig. 5. Rock type classification diagrams for intrusion from Gol Mod massif, Selenge Complex; a) Q-ANOR TAS diagram (Streckeisen and Le Maitre, 1979), b) TAS diagram, after (Middlemost, 1994), c) K_2O-SiO_2 diagram. Solid line is from (Peccerillo and Taylor, 1976), d) A/NK-A/CNK diagram. A/NK = Al/(Na+K) (molar ratio). A/ CNK = Al/(Ca+Na+K) (molar ratio) (Shand, 1943)

Table 1. Geochemical data of the whole rock for Gol Mod massif, Northern Mongolia

Lithogy	alkali granite	alkali granite	alkali granite	alkali granite	alkali granite	granite
Number	**GM-01**	**Gm-02**	**Gm-03**	**Gm-04**	**GM-05**	**Gm-06**
SiO_2	66.22	69.14	65.52	73.59	73.96	70.53
TiO_2	0.64	0.45	0.63	0.28	0.27	0.28
Al_2O_3	16.25	15.80	17.48	13.64	12.44	14.94
Fe_2O_3	2.85	1.43	1.99	1.64	2.17	1.49
FeO	2.54	1.10	1.05	0.37	1.93	1.42
MnO	0.07	0.03	0.05	0.03	0.03	0.07
MgO	0.52	0.25	0.40	0.20	0.35	0.47
CaO	0.79	0.88	1.21	0.55	0.48	2.30
Na_2O	5.38	4.88	5.14	4.09	3.92	3.98
K_2O	5.83	4.98	5.65	4.77	4.99	3.25
P_2O_5	0.18	0.09	0.22	0.06	0.06	0.09
LOI	0.35	0.32	0.15	0.28	0.23	0.57
Total	101.62	99.35	99.49	99.50	100.83	99.39
Mg#	15.37	15.73	20.07	16.19	13.85	23.28
A/CNK	0.98	1.05	1.04	1.06	0.98	1.05
Norm calculations						
Quartz	10.03	19.63	11.44	30.25	30.15	29.10
Orthoclase	34.45	29.43	33.39	28.19	29.49	19.21
Albite	45.52	41.29	43.49	34.61	33.17	33.68
Anorthite	2.74	3.78	4.57	2.34	1.61	10.82
Hypersthene	2.68	0.77	1.00	0.50	2.07	2.22
Magnetite	4.13	2.07	1.72	0.48	3.15	2.16
Ilmenite	1.22	0.86	1.20	0.53	0.51	0.53
Hematite	0.00	0.00	0.80	1.31	0.00	0.00
Apatite	0.43	0.21	0.52	0.14	0.14	0.21
Sum	101.21	98.05	98.12	98.34	100.29	97.93
Trace elements (ppm)						
Rb	129.00	137.34	120.31	223.41	221.00	71.53
Ba	1250.00	906.09	1188.53	477.76	366.00	1096.59
Th	6.20	12.23	7.52	41.05	10.60	7.71
U	1.37	2.46	1.81	5.59	3.90	0.98
Nb	19.00	23.82	24.36	11.72	9.00	8.16
Ta	6.00	1.42	1.33	1.07	3.00	0.40
La	79.20	42.51	58.44	40.80	42.80	24.11

Note: LOI= Loss on Ignition. FeO = All Fe calculated as Fe_2O_3. Mg# = molar ($MgO/(MgO + FeO^{2+})$) 100, assuming Fe^{2+}/Fe total=0.9. Normalizing factors after Sun and McDonough (1989). The less-than sign (<) indicates that the value is below the detection limit.

were used to illustrate the classification and discrimination diagrams for the rock units. The SiO_2 contents of second stage of granitoid and first stage of the gabbroid range from 65.52 to 73.96 wt % and from 47.5 to 56.86 wt %, respectively. Two types of rocks are classified as alkali feldspar granitoid and gabbroid in the Q-Anor TAS diagram (Streckeisen and Le Maitre, 1979) (Fig. 5a). In Na_2O+K_2O vs SiO_2 TAS diagram, these samples are plot in two various types as gabbro-monzodiorite and granodiorite and alkali feldspar granite (Fig. 5b), respectively. In the K_2O-SiO_2 diagram (Fig. 5c), these rocks are all plotted in high-K, calc-alkaline series. They are all displayed in the the metaluminous field in A/CNK vs. A/NK diagram (Fig. 5d). Second stage rocks have low MgO (0.2–0.52 wt %) contents with high Mg# (13.5-23.28) and first stage rocks have low MgO (2.77-6.26 wt %) contents with high Mg# (41.5-46.2) in Table 1. Except for K_2O, the major oxides (Al_2O_3, MgO, CaO, Na_2O, FeOt, P_2O_5 and TiO_2) show a decrease in their abundance with increasing silica in the granites (Fig. 6). The chondrite normalized REE diagram (Boynton, 1984) shows that all patterns of all stage rocks are strongly fractionated, showing the strong enrichment in LREE relative to HREEs with high (La/Yb)N (Fig. 7a). Slightly Eu negative anomalies are observed in these rocks. The primitive mantle normalized spider diagram (Sun and McDonough, 1989) shows that the all stage rocks are depleted in high field strength elements (HFSE) of Nb, Ti, Th, P and Y and enriched in Rb, Pb, U and K (Fig. 7b).

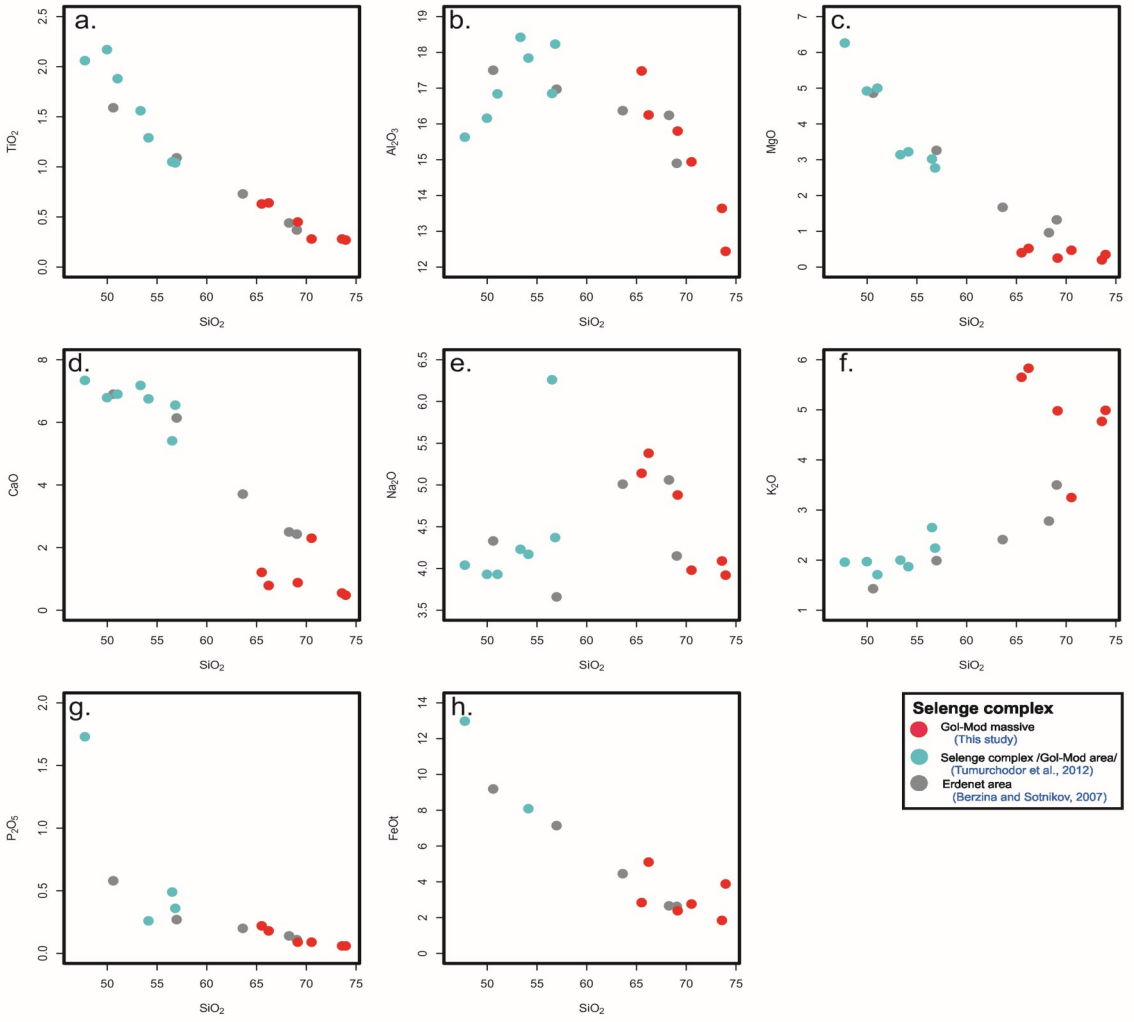

Fig. 6. Harker diagrams of major elements for the Selenge Complex

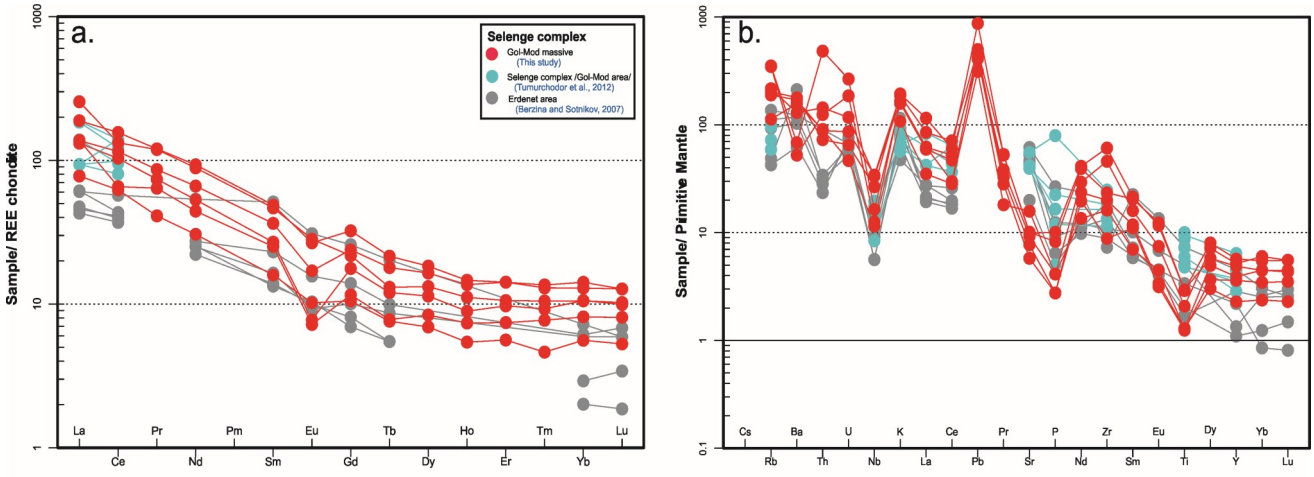

Fig. 7. a) Chondrite-normalized REE (normalizing values are from Boynton, 1984); b) Primitive mantle-normalized spider diagram (normalizing values are from Sun and McDonough, 1989); Data of the Selenge Complex: from first and final stage (Intermediate to mafic intrusive rocks from Tumurchudur et al. (2012), the second stage of Gol-Mod massif (Felsic intrusive rocks) (this study) and Selenge Complex of second stage from Berzina and Sotnikov (2007) in Erdenet area.

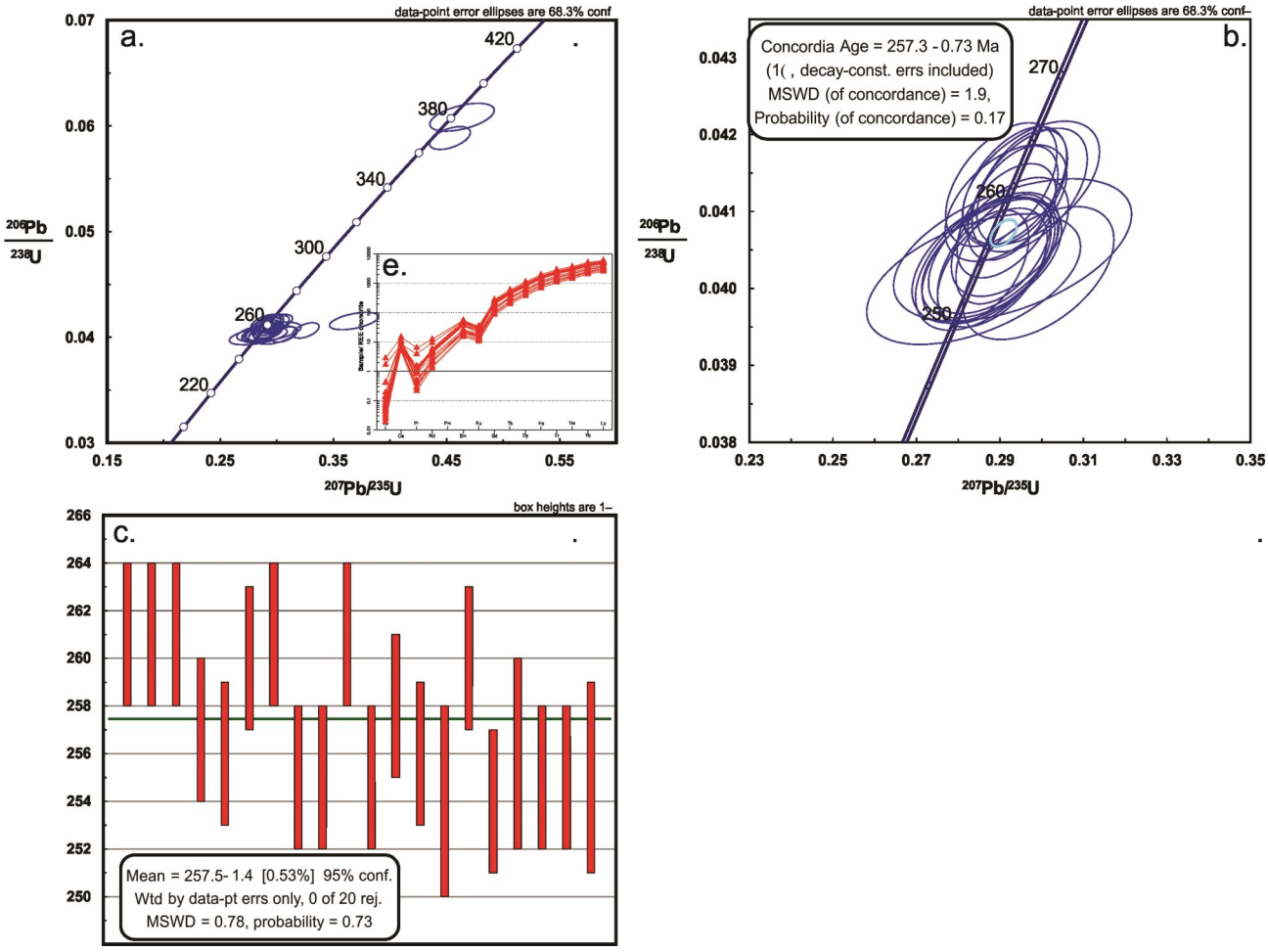

Fig. 8. a.b.c) Concordia diagrams, probability description plots and weighted mean ages for Gol Mod intrusive rock, Selenge Complex (MSWD: mean square weighted deviation).

Table 2. LA-ICP-MS zircon U–Pb analytical results from Gol Mod massif, Northern Mongolia

Sample		Isotopic ages (Ma)								Conc. (%)*
Spot	$^{238}U/^{232}Th$	$^{207}Pb/^{206}Pb$	±1σ	$^{207}Pb/^{235}U$	±1σ	$^{206}Pb/^{238}U$	±1σ	$^{208}Pb/^{232}U$	±1σ	
Alkaline granite (GM-05)										
M155-01	4.5661	278	34	263	6	261	3	265	5	0.7663
M155-02	2.8874	237	46	259	7	261	3	241	5	-0.7663
M155-03	3.5448	294	47	264	7	261	3	286	6	1.1494
M155-04	2.3599	291	49	260	7	257	3	269	5	1.1673
M155-05	4.6238	288	38	259	6	256	3	269	4	1.1719
M155-06	3.1242	272	34	261	6	260	3	258	4	0.3846
M155-07	2.244	263	42	261	6	261	3	252	4	0
M155-08	3.3037	272	65	257	9	255	3	262	6	0.7843
M155-09	2.926	261	68	256	9	255	3	236	6	0.3922
M155-10	3.2433	292	90	264	8	261	3	261	3	1.1494
M155-11	2.4915	261	36	255	6	255	3	254	4	0
M155-12	2.2132	424	65	387	13	381	5	352	8	1.5748
M155-13	4.3229	273	40	260	6	258	3	272	5	0.7752
M155-14	1.9857	752	89	318	11	262	3	256	3	21.374
M155-15	2.0704	533	32	286	6	257	3	258	4	11.284
M155-16	1.4911	273	58	257	8	256	3	269	4	0.3906
M155-17	0.7616	370	64	266	9	254	4	240	4	4.7244
M155-18	2.2576	259	53	260	8	260	3	285	5	0
M155-19	1.42	254	141	254	13	254	3	254	3	0
M155-20	2.2733	446	37	379	8	369	4	377	6	2.71
M155-21	1.6614	306	119	261	15	256	4	275	6	1.9531
M155-22	2.4686	281	46	257	7	255	3	262	5	0.7843
M155-23	5.2641	268	59	256	8	255	3	312	8	0.3922
M155-24	5.0861	260	60	255	8	255	4	274	7	0
M155-25	1.2698	422	35	272	6	254	3	270	4	7.0866

Table 3. Trace element (ppm) data for zircon crystals from the Gol Mod massif, Northern Mongolia

Sample Spot	Tm	Yb	La_N	Sm_N	Ce_N	Pr_N	EuN	GdN	$(Sm/La)_N$	Ce/Ce*	(Eu/Eu*)N	Ce(IV)/Ce(III)	T (°C)
Alkali granite (GM-05)													
1	2856.79	4046.56	0.05	43.03	7.18	1.05	27.85	222.7	860.6	31.34	0.28	16.23	671.44606
2	3288.58	4561.87	2.78	54.97	14.48	6.29	31.99	254.86	19.77	3.46	0.27	23.33	744.42685
3	2103.09	3021.72	0.13	26.51	5.94	0.84	18.68	139.58	203.92	17.98	0.31	27.42	651.12643
4	3058.64	4300.24	0.41	38.15	10.36	0.93	25.05	212.2	93.05	16.78	0.28	32.51	661.36494
5	2762.04	3864.59	0.06	42.51	5.47	1.15	27.32	207.41	708.5	20.82	0.29	11.98	650.21637
6	3647.53	5047.66	0.03	51.38	10.95	1.14	29.28	276.02	1712.67	59.21	0.25	21.71	622.28135
7	2708.95	3855.5	0.02	36	7.71	1.06	24.07	190	1800	52.95	0.29	24.33	666.83155
8	2918.83	4137.61	0.42	40.67	8.02	1.52	30.3	224.21	96.83	10.04	0.32	21.24	704.18315
9	2996.91	4185.5	0.07	41.85	5.5	1.13	30.46	224.94	597.86	19.56	0.31	13.46	643.31341
10	2066.98	2974.5	0.07	22.46	8.82	0.47	15.18	132.74	320.86	48.63	0.28	56.22	669.44467
11	2767.59	3913.25	0.03	38.1	7.09	0.96	25.07	204.86	1270	41.78	0.28	19.91	653.13977
12	2027.78	2923.35	0.07	23.79	7.7	0.49	17.37	132.43	339.86	41.58	0.31	42.89	716.81575
13	2350.62	3365.26	0.07	25.64	13.7	0.47	14.87	154.02	366.29	75.53	0.24	75.44	670.90459
14	3235.19	4536.75	1.67	52.56	8.28	3.84	33.61	256.49	31.47	3.27	0.29	14.02	656.18188
15	3336.73	4654.98	0.07	48.41	8.97	1.19	29.43	251.66	691.57	31.08	0.27	18.66	701.86752
16	1712.35	2532.25	0.05	20.51	6.31	0.26	14.67	109.96	410.2	55.34	0.31	41.74	684.1934
17	2748.46	3908.71	0.19	36.46	7.14	1.17	20.31	195.21	191.89	15.14	0.24	22.76	688.33143
18	1586.42	2293.3	0.02	17.03	5.51	0.38	12.23	98.88	851.5	63.2	0.3	48.34	685.12886
19	1774.38	2589.09	0.04	20.1	5.83	0.39	14.3	110.39	502.5	46.68	0.3	41	686.05508
20	1418.83	2064.26	0.06	15.23	5	0.21	10.57	86.25	253.83	44.54	0.29	49.82	684.34996
21	3051.54	4250.29	0.1	44.26	5.35	1.35	28.52	233.17	442.6	14.56	0.28	11.76	642.56639
22	3064.51	4310.96	0.08	46.77	4.94	1.19	34.97	251.81	584.63	16.01	0.32	9.65	707.06445
23	3146.6	4447.89	0.08	43.49	7.92	1.19	28.86	236.8	543.63	25.67	0.28	19.17	674.62884
24	2709.57	3816.46	0.08	37.38	5.16	0.89	24.42	194.79	467.25	19.34	0.29	14.68	672.69706
25	1597.53	2317.42	0.14	16.77	5.63	0.29	12.75	94.29	119.79	27.94	0.32	51.05	683.87949

Note: Ce/Ce*= $\{CeN/((LaN \times PrN)^{1/2}\}$ and Eu/Eu*= $\{EuN/((SmN \times GdN)^{1/2}\}$, where the subscript (N) indicates chondrite normalization. Chondrite values are from Boynton (1984). The T(°C) was calculated by using the Ti-in-zircon thermometer of Watson et al. (2006)

Zircon U-Pb geochemistry

Zircon U-Pb isotope data of analyzed zircons for one sample are listed in Table 2 and 3. The zircon U-Pb Concordia diagrams are shown in Fig. 8. The geological age was obtained on the basis of acceptable results from a probability density plot, a tight filter of concordant ages and the mean age calculation for sample. The zircon crystallization temperatures are average (622°-744°C) that listed in Table 3 (Watson et al., 2006). Among the twenty-five zircon grains (25 points) ablated from the alkali feldspar granite sample (GM-05) (Fig. 8a), 20 were concordant. Twenty analyses were grouped tightly and defined a Concordia age of 257.3 ± 0.73 Ma (Fig. 8b), which was found to be consistent with the weighted mean $^{206}Pb/^{238}U$ age of 257.5±1.4 Ma (MSWD=0.78; Fig. 8c) which is accepted as the best estimate of crystallization age.

Zircon Geochemistry

The zircon grains were analyzed for 25 trace elements (e.g., P, Ca, Ti, Y, Nb, REE, Hf, Ta, Pb, Th, and U). The results of the trace element analyses and related parameters are listed in Table 2. The zircons possessed relatively low LREE patterns with pronounced positive Ce and small negative Eu anomalies (Fig. 7). It has been popularly accepted that the magnitude of depleted Eu and Ce abundances depends on the oxidation state during the mineral crystallization (Hoskin and Schaltegger, 2003; Trail et al., 2012). The discrimination diagrams of zircons are given in Fig. 9. The origin of zircons can be magmatic or non-magmatic, which can be recognized by their morphology, zoning, and trace element geochemistry (e.g., Belousova et al., 2002; Fu et al., 2009; Grimes et al., 2007; Hoskin, 2005). Considering these

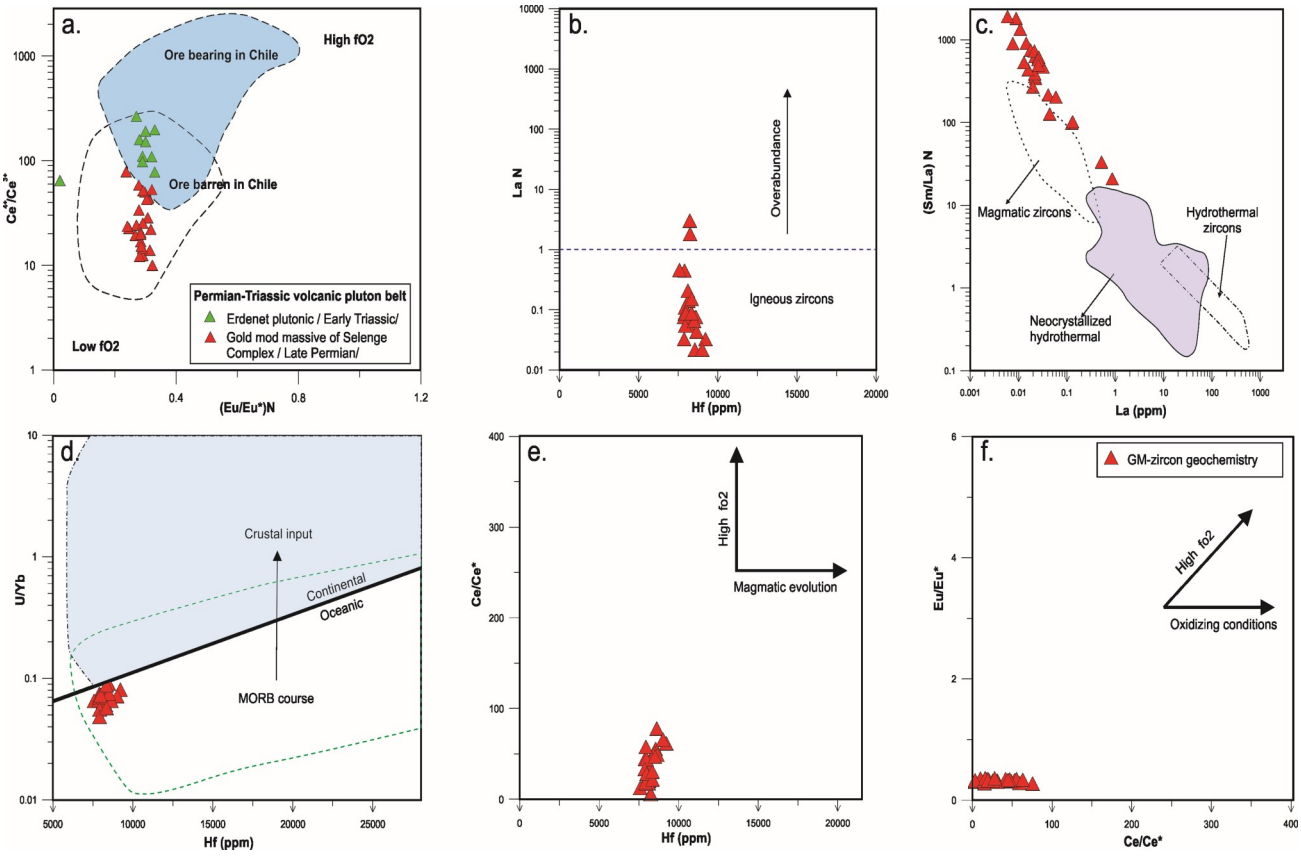

Fig. 9. Zircon trace element discrimination diagrams: a) (Sm/La)N vs. La diagram, fields of magmatic and hydrothermal zircons are from Grimes et al., (2009) and Hoskin, (2005), while hydrothermally recrystallized field adopted from Kirkland et al., (2009); b) LaN vs. Hf, Igneous zircon fields data are from Hoskin and Schaltegger (2003); c) (Eu/Eu*)N vs. Ce^{4+}/Ce^{3+} diagram. The area of ore barren and ore bearing rocks in Chile is from Ballard et al. (2002), Green filled triangular circles are from Erdenet pluton of ore bearing intrusion (Shen et al., 2015); d) Ce/Ce* vs. Hf;; e) Eu/Eu* vs. Ce/Ce; f) U/Yb vs. Hf, the values of continental and ocean crust (arc magmatism) zircons are from Grimes et al. (2007)

parameters and their ages, mainly one type of zircons (magmatic) is identified from the studied sample.

DISCUSSION

Significance of Magmatic Zircon

All magmatic zircons were found to contain detectable amounts of the HFSE (Table 3), which fell within the normal abundance of magmatic zircons (Ti 75 ≤ppm, Nb ≤ 62 ppm, Ta> 3 ppm) (Hoskin and Schaltegger, 2003). The crystallization temperatures of zircons fit well with magmatic zircons ($T_{Ti\text{-}in\text{-}zrc}$ > 550 °C) (Table 3; Fu et al., 2009). As shown in Fig. 9a, they mostly demonstrated high $(Sm/La)_N$ associated with low La, that is representative of the unaltered magmatic zircons (Hoskin, 2005; Grimes et al., 2009). In addition, they mainly showed igneous zircons in the La_N versus Hf diagram (Fig. 9b). Therefore, the redox state of rocks was conventionally related to the oxygen fugacity of the magma. The Hf vs. Ce/Ce* diagram (Fig. 9d) shows that all zircons plotted mainly in a limited range of oxygen fugacity with slightly progressive magma evolution, thereby indicating that they were primarily crystallized under relatively reduced environments (low fO_2). The Ce/Ce* vs. Eu/Eu* diagram is also very useful in revealing the redox conditions under which the magma was formed (Trail et al., 2012). All of the magmatic zircons from studied units displayed an anti-correlation trend along the direction of oxidizing conditions (Figs. 9d. e).

We also obtained oxygen fugacity from zircon by using Ce^{4+}/Ce^{3+} vs. $(Eu/Eu^*)_N$ diagram (Fig. 9c; Ballard et al., 2002). They were found to lie on the polygon of low fO_2 thus confirming their formation under low oxygen fugacity. Therefore, high fO_2 magmas are widely discovered in the Early Triassic (Ore bearing Erdenet pluton) of the Late Permian to Early Triassic volcanic-plutonic belt.

Implication for the Tectonic Setting

The Selenge volcano-plutonic belt located in the north-western Mongol-Okhotsk Belt which is closely related to mineralization, is a composite intrusion. The oldest Selenge pluton (277–253 Ma) consists of calc-alkaline shoshonite-latite rocks, and coeval volcanics (Munkhtsengel et al., 2007). The younger 240 Ma quartz-diorite yielded εHf(t) values from +6.9 to +14.8 and tHf(DM) ages between 830 and 320 Ma (Ganbat et al., 2021). The Triassic magmatic activity formed alkaline intrusions and bimodal igneous series different from older subduction-related magmas (Munkhtsengel et al., 2007). Ore-bearing Erdenet intrusions yielded ages of 245–235 Ma, and Re–Os in molybdenite yielded an age of 240 Ma (Morozumi, 2003). The Permian to Triassic igneous rocks of northern Mongolia belong to two age complexes: early subduction-collision and late rift (Litvinovsky et al., 1990; Yarmolyuk and Kovalenko, 1991). Therefore, the Selenge Complex pluton was yielded as K-Ar dates ranging from 290-260 Ma (Sotnikov et al., 1995).

From our LA-ICP-MS zircon U–Pb isotope data alkali feldspar granite yielded a Concordia age of 257.3±0.73 Ma in the the Gol Mod massif of the Late Permian. The 257.3 Ma intrusive was previously weak considered as Late Permian to Early Triassic period (Tumurchudur et al., 2012), but our new data reveal that it has Late Permian age. The magmatic history that includes the Selenge Complex is as follows: Early Permian bimodal volcanism of trachybasalt-trachyandesite and rhyolite-trachyrhyolite started in the northern Mongolian magmatic belt, and this volcanism was followed by Late Permian granite, syenogranite, syenite, and gabbroid plutonic (Dejidmaa and Naito, 1998). We suggest that the Gol Mod massif is almost coeval and related to the Selenge pluton (Erdenet ore district area) as they possess similar geochemical characteristics and show slightly different ages of crystallization and mineralization.

On the tectonic discrimination diagram of zircon U/Yb versus Hf diagram (Fig. 9f) and whole rock Ta versus Y and Rb vs Ta+Yb diagram (Figs. 10a, b), the Gol Mod massif plots in the field of arc magmatism and volcanic arc granite (VAG) and syn-collision granite (syn-COLG). Also, on the Th/Yb vs Nb/Yb diagram, that plot in the field of continental arcs (CA) (Fig. 10c). The Gol Mod

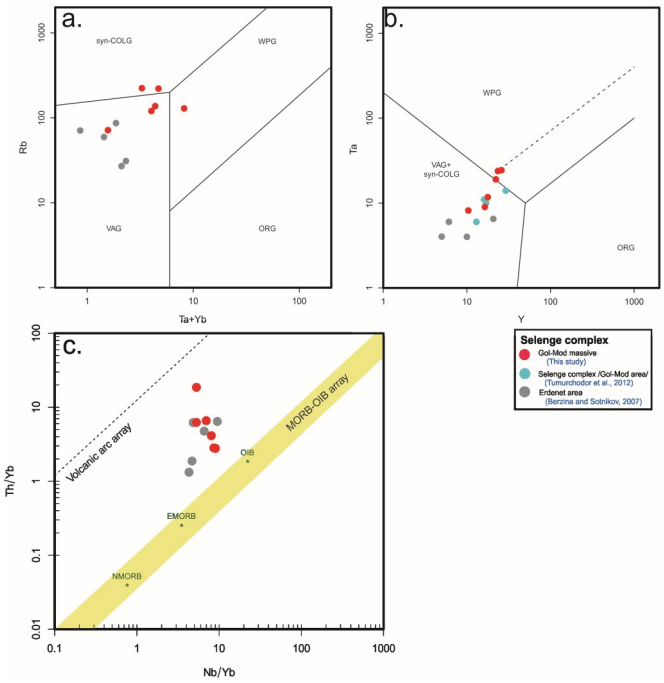

Fig.10. Tectono-magmatic discrimination diagrams of Gol Mod intrusive rocks. a, b) Ta + Yb vs Rb and Y vs Ta (Pearce et al., 1984); c) Th/Yb vs. Nb/Yb (Pearce, 2014)

massif occurred during the latest stage of northern Mongolian arc magmatism, which was followed by Late Permian subduction-collision between the Mongolian- North China and Siberian blocks (Gusev and Khain, 1995; Gerel, 1998; Berzina et al., 1999). In addition, our new data provide a significant piece to solve the magmatic evolution of the south-western part of the Orkhon-Selenge volcanic plutonic belt and north-western part of Mongol-Okhotsk plate during the Late Paleozoic -Early Mesozoic period.

CONCLUSION

The Gol Mod massif is emplaced 257.3 ± 0.73 Ma that composed mainly of alkali feldspar granite and granodiorite of south-western part of the Selenge Complex in the Late Permian period, north-western Mongolia.

The intrusive rocks have varieties depleted and enriched in REE and trace elements. The former varieties are similar in geochemical characteristics with gabbroid of the Gol Mod area (Tumurchudur et al., 2012) and the Selenge Complex of the Erdenet area (Berzina and Sotnikov, 2007) that the majority are plotted in a high calc-alkaline, I-type and subduction-related continental arc environment.

The formation of south-western part of the Selenge Complex (Gol Mod massif) was accompanied by the production of poor mineralization due to it has a low oxygen fugacity of zircon (fO_2) and the ore elements of the granitoids might have been later extracted by the porphyry magma, which increased its ore potential under high oxygen fugacity (fO_2) in the Late Triassic Erdenet Pluton. These granitoids are emplaced in Late Permian to Early Triassic volcanic plutonic belt.

ACKNOWLEDGEMENTS

The study was supported by a grant 20-55-44002-Mong_a from the Russian Foundation for Basic Research. We are grateful to the Geology Department (Institute of Geology, Mongolian Academy of Science, Mongolia) and the Vinogradov Institute of Geochemistry SB RAS, Irkutsk, Russia. We are also indebted to Mr. S. Turbold for zircon U-Pb isotopes analysis of the Key Laboratory of Orogeny and Crust Evolution (Peking University) and for geochemistry analysis of the Center of Isotope-geochemical Studies, Vinogradov Institute of Geochemistry, Siberian Branch of the Russian Academy of Sciences (IGS SB RAS).

REFERENCES

Andersen, T. 2002. Correction of common lead in U–Pb analyses that do not report 204Pb: Chemical Geology, v. 192, p. 59-79. https://doi.org/10.1016/S0009-2541(02)00195-X

Badarch, G., Cunningham, D.W., Windley, B.F. 2002. A new terrane subdivision for Mongolia: Implications for the Phanerozoic crustal growth of Central Asia. Journal of Asian Earth Sciences, v. 21(1), p. 87-110. https://doi.org/10.1016/S1367-9120(02)00017-2

Ballard, J.R., Palin, M.J., Campbell, I.H. 2002. Relative oxidation states of magmas inferred from Ce (IV)/Ce (III) in zircon: application to porphyry copper deposits of northern Chile. Contributions to Mineralogy and Petrology, v. 144, p. 347-364. https://doi.org/10.1007/s00410-002-0402-5

Belousova, E.A., Griffin, W.L., O'Reilly, S.Y.,

Fisher, N.L. 2002. Igneous zircon: trace element composition as an indicator of source rock type. Contributions to Mineralogy and Petrology, v. 143, p. 602-622. https://doi.org/10.1007/s00410-002-0364-7

Berzina, A.N., Sotnikov, V.I., Ponomarchuk, V.A., Berzina, A.P., Kiseleva, V.Y., Stanley, C.J. 1999. Temporal periods of formation of Cu-Mo porphyry deposits, Siberia and Mongolia. Mineral deposits -Processes to Processing. Rotterdam, Balkema, p. 321-324.

Berzina, A.P., Sotnikov, V.I. 2007. Character of formation of the Erdenet-Ovoo porphyry Cu-Mo magmatic center (northern Mongolia) in the zone of influence of a Permo-Triassic plume. Russian Geology and Geophysics, v. 48, p. 141-156. https://doi.org/10.1016/j.rgg.2007.01.001

Boynton, W.V. 1984. Cosmochemistry of the rare earth elements: meteorite studies, in: Developments in Geochemistry. Elsevier, v. 2, p. 63-114. https://doi.org/10.1016/B978-0-444-42148-7.50008-3

Dejidmaa, G., Naito, K. 1998. Previous studies on the Erdenetiin ovoo porphyry copper-molybdenum deposit, Mongolia (特集 **モンゴル国の鉱物資源**). Bulletin of the Geological Survey of Japan, v. 49(6), p. 299-308.

Fu, B., Mernagh, T.P., Kita, N.T., Kemp, A.I.S., Valley, J.W. 2009. Distinguishing magmatic zircon from hydrothermal zircon: A case study from the Gidginbung high-sulphidation Au–Ag–(Cu) deposit, SE Australia. Chemical Geology, v. 259(3-4), p. 131-142. https://doi.org/10.1016/j.chemgeo.2008.10.035

Ganbat, A., Tsujimori, T., Miao, L., Safonova, I., Pastor-Galán, D., Anaad, C., Baatar, M., Aoki, S., Aoki, K., Savinskiy, I. 2021. Late Paleozoic–Early Mesozoic granitoids in the Khangay-Khentey basin, Central Mongolia: Implication for the tectonic evolution of the Mongol-Okhotsk Ocean margin. Lithos, v. 404-405. https://doi.org/10.1016/j.lithos.2021.106455

Gerel, O. 1998. Phanerozoic felsic magmatism and related mineralization in Mongolia (特集 **モンゴル国の鉱物資源**). **地質調査所月報**, v. 49(6), p. 239-248.

Gerel, O., Dandar, S., Amar-Amgalan, S., Javkhlanbold, D., Myagamarsuren, S., Myagmarsuren, S., Munkhtsengel, B., Soyolmaa, B. 2005. Geochemistry of granitoids and altered rocks of the Erdenet porphyry copper-molybdenum deposit, central Mongolia. Mineral Deposit Research: Meeting the Global Challenge, Springer, p. 1137-1140. https://doi.org/10.1007/3-540-27946-6_290

Govindaraju, K. 1994. 1994 compilation of working values and sample description for 383 geostandards. Geostandards Newsletter, v. 18, p. 1-158. https://doi.org/10.1007/s00410-009-0409-2

Grimes, C.B., John, B.E., Cheadle, M.J., Mazdab, F.K., Wooden, J.L., Swapp, S., Schwartz, J.J. 2009. On the occurrence, trace element geochemistry, and crystallization history of zircon from in situ ocean lithosphere. Contributions to Mineralogy and Petrology, v. 158(6), p. 757-783. https://doi.org/10.1007/s00410-009-0409-2

Grimes, C.B., John, B.E., Kelemen, P.B., Mazdab, F.K., Wooden, J.L., Cheadle, M.J., Hanghøj, K., Schwartz, J.J. 2007. Trace element chemistry of zircons from oceanic crust: A method for distinguishing detrital zircon provenance. Geology, v. 35(7), p. 643-646. https://doi.org/10.1130/G23603A.1

Gurragchaa, I., Төмөртогоо, О. 2014. UGZ-geological map 1:200 000, M-47-XXXVI.

Gusev, G.S., Khain, V.Y. 1995. On relations between the Baikal-Vitim, Aldan-Stanovoy, and Mongol-Okhotsk terranes (south of mid-Siberia). Geotectonics, v. 29(5), p. 422–436.

Hanžl, P., Guy, A., Battushig, A., Lexa, O., Schulmann, K., Kunceová, E., Hrdličková, K., Janoušek, V., Buriánek, D., Krejčí, Z., Jiang, Y., Otgonbaatar, D. 2020. Geology of the Gobi and Mongol Altai junction enhanced by gravity analysis: a key for understanding of the Mongolian Altaides. Journals of Maps, v. 16(2), p. 98-107. https://doi.org/10.1080/17445647.2019.1700835

Hoskin, P.W.O. 2005. Trace-element composition of hydrothermal zircon and the alteration of Hadean zircon from the Jack Hills, Australia. Geochimica et Cosmochimica Acta, v. 69(3), p. 637-648. https://doi.org/10.1016/j.gca.2004.07.006

Hoskin, P.W.O., Schaltegger, U. 2003. The composition of zircon and igneous and metamorphic petrogenesis. Reviews in Mineralogy and Geochemistry, v. 53(1), p. 27-62. https://doi.org/10.2113/0530027

Jahn, B., Wu, F., Chen, B. 2000. Granitoids of the Central Asian Orogenic Belt and continental growth in the Phanerozoic. Earth and Environmental Science Transactions of The Royal Society of Edinburgh, v. 91(1-2). p. 81-193. https://doi.org/10.1017/S0263593300007367

Kirkland, C.L., Whitehouse, M.J., Slagstad, T. 2009. Fluid-assisted zircon and monazite growth within a shear zone: a case study from Finnmark, Arctic Norway. Contributions to Mineralogy and Petrology, v. 158(5), p. 637-657. https://doi.org/10.1007/s00410-009-0401-x

Litvinovsky, B.A., Podladtchikov, Y.Y., Zanvilevitch, A.N., Dunitchev, V.M. 1990. On the melting of acidic volcanites in the contact of basic magma at shallow depth. Geokhimiya v. 6, p. 807-814 (in Russian).

Ludwig, K.R. 2003. User's manual for isoplot 3.00, a geochronlogical toolkit for microsoft excel. Berkeley Geochronology Center. Special Publication, No 4, p. 25-32.

Middlemost, E.A.K. 1994. Naming materials in the magma/igneous rock system. Earth Science Reviews, v. 37, p. 215-224. https://doi.org/10.1016/0012-8252(94)90029-9

Morozumi, H. 2003, Geochemical characteristics of granitoids of the Erdenet porphyry copper deposit, Mongolia. Resource Geology, v. 53, p. 311-316. https://doi.org/10.1111/j.1751-3928.2003.tb00180.x

Munkhtsengel, B., Gerel, O., Tsuchiya, N., Ohara, M. 2007. Petrochemistry of Igneous Rocks in Area of the Erdenetiin Ovoo Porphyry Cu-Mo Mineralized District, Northern Mongolia, in AIP Conference Proceedings, American Institute of Physics, v. 898, p. 63-65. https://doi.org/10.1063/1.2721250

Pearce, J.A. 2014. Immobile element fingerprinting of ophiolites. Elements, v. 10 (2), p. 101-108. https://doi.org/10.2113/gselements.10.2.101

Pearce, J.A., Harris, N.B.W., Tindle, A.G. 1984. Trace element distribution diagrams for the tectonic interpretation of granitic rocks. Journal of Petrology. v. 25(4), p. 956-983. https://doi.org/10.1093/petrology/25.4.956

Peccerillo, A., Taylor, S.R. 1976. Geochemistry of Eocene calc-alkaline volcanic rocks from the Kastamonu area, northern Turkey. Contributions to Mineralogy and Petrology, v. 58, p. 63-81. https://doi.org/10.1007/BF00384745

Şengör, A.M.C., Natal'In, B.A., Burtman, V.S. 1993. Evolution of the Altaid tectonic collage and Palaeozoic crustal growth in Eurasia. Nature, v. 364, p. 299-307. https://doi.org/10.1038/364299a0

Shand, S.J. 1943. Eruptive Rocks. Their Genesis, Composition, Classification, and Their Relation to Ore-Deposits with a Chapter on Meteorite. New York: John Wiley & Sons.

Shen, P., Hattori, K., Pan, H., Jackson, S., Seitmuratova, E. 2015. Oxidation condition and metal fertility of granitic magmas: Zircon trace-element data from porphyry cu deposits in the Central Asian Orogenic Belt. Economic Geology, v. 110(7), p. 1861-1878. https://doi.org/10.2113/econgeo.110.7.1861

Sotnikov, V.I., Ponomarchuk, V.A., Berzina, A.P., Travin, A.V. 1995. Geochronological borders of magmatism of Cu-Mo-porphyry Erdenetuin-Obo deposit (Mongolia). Geologiya i Geofizika, v. 36(3); p. 78-89.

Streckeisen, A., Le Maitre, R.W. 1979. A chemical approximation to the modal QAPF classification of igneous rocks: Neues Jahrbuch für Mineralogie Abhandlugen, v. 136, p. 169-206.

Sun, S.S., McDonough, W.F. 1989. Chemical and isotopic systematics of oceanic basalts: Implications for mantle composition and processes. Geological Society, London, Special Publications, v. 42, p. 313-345. https://doi.org/10.1144/GSL.SP.1989.042.01.19

Tang, J., Xu, W.-L., Wang, F., Zhao, S., Wang, W. 2016. Early Mesozoic southward subduction history of the Mongol-Okhotsk oceanic plate: Evidence from geochronology and geochemistry of Early Mesozoic intrusive rocks in the Erguna Massif, NE China: Gondwana Research, v. 31, p. 218-240. https://doi.org/10.1016/j.gr.2014.12.010

Trail, D., Watson, E.B., Tailby, N.D. 2012. Ce

and Eu anomalies in zircon as proxies for the oxidation state of magmas. Geochimica et Cosmochimica Acta, v. 97, p. 70-87. https://doi.org/10.1016/j.gca.2012.08.032

Tumurchudur, C., Ganbayar, G., Ariunbold, P. 2012. 1:50,000 scale geological mapping, general prospecting of the Khunuin Gol area. Geological Information Center of Mongolia, Report #7055.

Watanabe, Y., Stein, H.J. 2000. Re-Os ages for the Erdenet and Tsagaan Suvarga porphyry Cu-Mo deposits, Mongolia, and tectonic implications. Economic Geology, v. 95, p. 1537-1542. https://doi.org/10.2113/95.7.1537

Watson, E.B., Wark, D.A., Thomas, J.B. 2006. Crystallization thermometers for zircon and rutile. Contributions to Mineralogy and Petrology, v. 151, p. 413-433. https://doi.org/10.1007/s00410-006-0068-5

Windley, B.F., Alexeiev, D., Xiao, W., Kroner, A., Badarch, G. 2007. Tectonic models for accretion of the Central Asian Orogenic Belt. Journal of the Geological Society, v. 164, p. 31–47. https://doi.org/10.1144/0016-76492006-022

Yarmolyuk, V.V, Kovalenko, V.I. 1991. Rift magmatism of active continental margins and its ore potential. Nauka, Moscow (in Russian).

Yarmolyuk, V.V., Kozlovsky, A.M., Savatenkov, V.M., Kovach, V.P., Kozakov, I.K., Kotov, A.B., Lebedev V.I., Eenjin, G. 2016. Composition, sources, and geodynamic nature of giant batholiths in Central Asia: evidence from the geochemistry and Nd isotopic characteristics of granitoids in the Khangai Zonal magmatic area. Petrology, v. 24, p. 433-461. https://doi.org/10.1134/S0869591116050064

Zhao, P., Xu, B., Jahn, B.M. 2017. The Mongol -Okhotsk Ocean subduction-related Permian peraluminous granites in northeastern Mongolia: Constraints from zircon U-Pb ages, whole-rock elemental and Sr-Nd-Hf isotopic compositions: Journal of Asian Earth Sciences, v. 144, p. 225-242. https://doi.org/10.1016/j.jseaes.2017.03.022

Zonenshain, L.P., Kuzmin, M.I., Natapov, L.M. 1990. Benjamin M.P. (Ed). Geology of the USSR: Plate-Tectonic Synthesis. Geodynamics Series Volume 21. ISBN 0-87590-521-8. https://doi.org/10.1029/GD021

Zorin, Y.A. 1999. Geodynamics of the western part of the Mongolia–Okhotsk collisional belt, Trans-Baikal region (Russia) and Mongolia: Tectonophysics, v. 306, p. 33-56, https://doi.org/10.1016/S0040-1951(99)00042-6